

Ferroelectric valley valves with graphene/MoTe₂ van der Waals heterostructures

Adolfo O. Fumega¹ and Jose L. Lado¹

¹*Department of Applied Physics, Aalto University, 02150 Espoo, Finland*

Ferroelectric van der Waals heterostructures provide a natural platform to design a variety of electrically controllable devices. In this work, we demonstrate that AB bilayer graphene encapsulated in MoTe₂ acts as a valley valve that displays a switchable built-in topological gap, leading to ferroelectrically driven topological channels. Using a combination of *ab initio* calculations and low energy models, we show that the ferroelectric order of MoTe₂ allows the control of the gap opening in bilayer graphene and leads to topological channels between different ferroelectric domains. Moreover, we analyze the effect that the moiré modulation between MoTe₂ and graphene layers has in the topological modes, demonstrating that the edge states are robust against moiré modulations of the ferroelectrically-induced electric potential. Our results put forward ferroelectric/graphene heterostructures as versatile platforms to engineer switchable built-in topological channels without requiring an external electric bias.

I. INTRODUCTION

Layered van der Waals compounds have become a fertile platform to engineer materials with emergent functionalities,¹ ranging from fundamental quantum states²⁻⁴ to nanoelectronic devices including field effect transistors⁵⁻⁷ and valves.⁸⁻¹⁰ The weak van der Waals bonding between layers allows to combine different monolayers with lattice constants, and to impose a rotation between the materials. This flexibility permits to use 2D building blocks with different symmetry-breaking orders: ferromagnets,¹¹⁻¹⁵ superconductors,¹⁶ ferroelectrics¹⁷ or multiferroics,^{18,19} that can be wisely merged to create heterostructures with promising applications. Paradigmatic examples of such combinations of different electronic orders are graphene/ferromagnet heterostructures realizing van der Waals tunnel junctions and valley polarization,²⁰⁻²³ graphene/semiconductor heterostructures leading to strong spin-orbit coupling effects,^{24,25} ferromagnet/superconductor heterostructures realizing topological superconductivity,^{26,27} ferromagnet/semiconductor providing controllable excitons,^{28,29} magnet/metal realizing heavy-fermion states,^{30,31} and ferroelectric/twisted bilayers realizing ferroelectrically switchable superconductivity.³² In particular, 2D ferroelectrics^{33,34} provide versatile building blocks to design valves that allow controlling the electronic properties of van der Waals heterostructures.^{32,35-37}

Graphene multilayers provide a flexible family of heterostructures to realize correlated, superconducting, and topological states.³⁸⁻⁴² In the particular case of AB-stacking bilayer graphene, an electric bias between the layers opens an energy gap, leading to an electrically-tunable gap semiconductor,⁴³⁻⁴⁷ and to a superconducting state in the slightly doped regime⁴⁸. At half-filling, the valleys at K and K' carry a momentum-space Berry curvature with opposite sign due to the broken inversion symmetry that occurs in this gapped system, thus displaying a valley Hall insulator behavior.⁴⁹⁻⁵² This phenomenon has been exploited to create topological edge

modes in the junction between oppositely gated regions⁵³ and also in AB-BA stacking domain walls.⁵⁰ In the absence of valley mixing, these chiral modes are topologically protected against back-scattering and present a ballistic transport.^{54,55} While such phenomena have been induced by an external bias, ferroelectric-based van der Waals heterostructures would lead to intrinsically persistent topological channels driven by the ferroelectric order. The control on the ferroelectric domains of the Valley Hall valve realized in such heterostructure would allow generating and tuning topological excitations. Therefore, it would provide a promising platform to print circuits displaying ballistic behavior.

In this work, we demonstrate, using a combination of *ab initio* calculations and low-energy models, the emergence of a valley valve in MoTe₂/bilayer graphene/MoTe₂ van der Waals heterostructures. The ferroelectric order of MoTe₂ gives rise to a built-in electrostatic bias in bilayer graphene, controllable by the orientation between the two MoTe₂ layers. In particular, the relative orientation of the ferroelectric order in MoTe₂ allows switching on and off the electronic gap of bilayer graphene and controlling its topological gap. In the insulating regime, topological states emerge in the boundary between opposite ferroelectric domains. We analyze the effect of the moiré modulation in the interlayer potential driven by the mismatch and potential twist between graphene and MoTe₂. Our results show that MoTe₂/graphene heterostructures realize robust valley topological modes in the presence of moiré modulations, thus putting forward a promising platform to obtain a ferroelectric valley valve with electrically-controlled topological excitations.

II. RESULTS AND DISCUSSION

We start demonstrating using *ab initio* first principles methods that bilayer graphene encapsulated in MoTe₂ displays a controlled gap driven by the ferroelectric order. Then, we will analyze with a low energy model the emergence of topological excitations in the boundary between two ferroelectric domains and their robustness

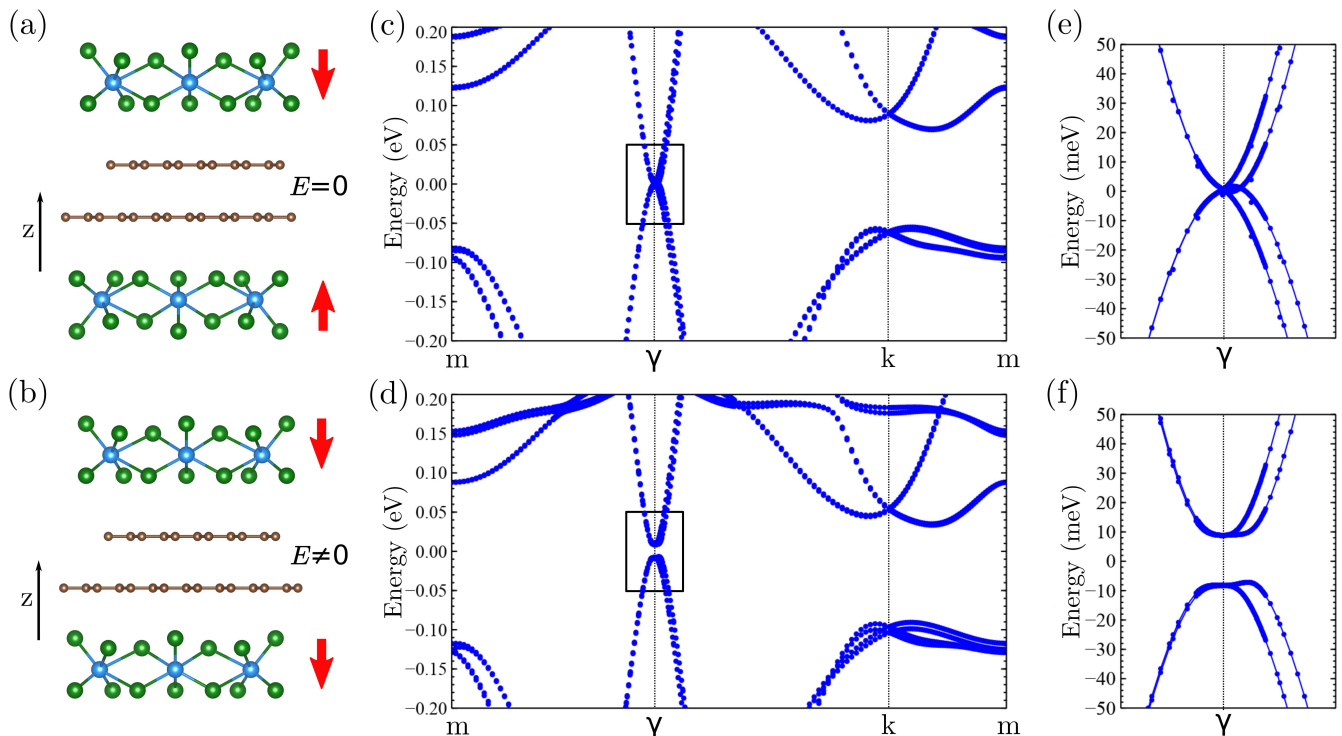


FIG. 1. (a,b) Structures of AB bilayer graphene encapsulated in ferroelectric MoTe₂ used in DFT calculations. In configuration (a), the ferroelectric order in MoTe₂ leads to a net zero electric field in the graphene bilayer, while in configuration (b) the ferroelectric proximity of the encapsulation leads to a non-zero electric field. The red arrows show the direction of the ferroelectric polarization in each of the MoTe₂ layers. C, Mo, and Te atoms are depicted in brown, blue, and green respectively. (c,d) Band structure calculations for the structures that are shown in panels (a) and (b) respectively. In panel (c) no energy gap opens as the net electric field is zero, while in panel (d) an energy gap opens up due to the net electric field induced in the graphene bilayer. Panels (e) and (f) show the zoomed areas near the Fermi level depicted as rectangles in panels (c) and (d) respectively.

against the moiré modulations induced by the mismatch between MoTe₂ and graphene.

A. Ab initio calculations

MoTe₂ shows a ferroelectric order with an out-of-plane electric polarization in the distorted d1T phase, which has been proven to be stable in MoTe₂/graphene heterostructures.¹⁷ We will exploit these properties to create a van der Waals heterostructure in which an electrically-controlled valley valve emerges. Our heterostructure consist of monolayer MoTe₂, Bernal-stacked AB graphene, and monolayer MoTe₂ as shown in Fig. 1ab. Figures 1a and 1b show the two possible configurations of the ferroelectric heterostructure that determine the valve. In the first configuration, the electric polarization of each of the MoTe₂ layers can be oriented in opposite direction leading to a zero electric field $E = 0$ in the heterostructure (Fig. 1a). In the second configuration, the electric polarizations of the MoTe₂ layers point in the same direction producing a non-zero electric field $E \neq 0$ in the heterostructure that can be felt by the graphene bilayer (Fig. 1b).

We now analyze the electronic structure of both configurations using first-principles density functional theory (DFT).⁵⁶ To create a computationally affordable heterostructure, we have commensurated this lattice parameter a with a 3×3 supercell for graphene and fix $a = 7.38$ Å.⁵⁷ DFT calculations are performed with QUANTUM ESPRESSO.^{58,59} These calculations were converged concerning all parameters in a 12×12 k -mesh and introducing a vacuum of 20 Å in the z -direction to ensure that there is not interaction of the heterostructure with neighboring unit cells in the z -direction.

Figures 1c and 1d show the corresponding band structures for both configurations of the heterostructure (Figs. 1a and 1b respectively). We can see in Fig. 1c, corresponding to the configuration with $E = 0$, that the electronic structure of the graphene bilayer remains gapless. This can be better seen in Fig. 1e which corresponds to a zoom of the rectangular area in Fig. 1c. Nevertheless, the band structure for the configuration with $E \neq 0$ displays a different behavior. We can see in Fig. 1d that an energy gap opens at the Fermi level as a consequence of the ferroelectric-induced field in the z -direction felt by the graphene bilayers. In the zoomed band structure (Fig. 1f) we can observe more clearly the induced gap,

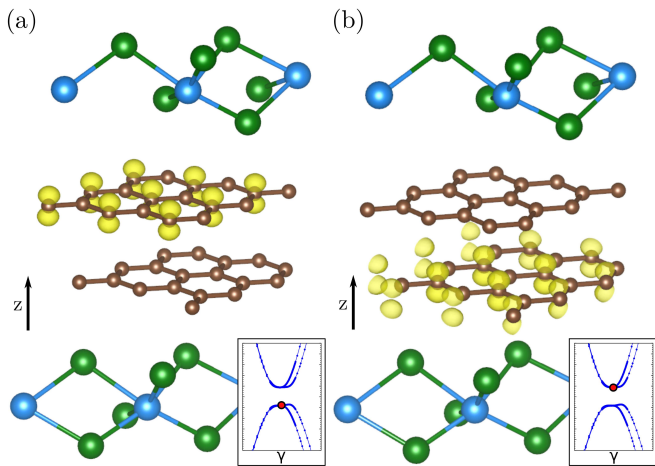


FIG. 2. Wavefunction probability density (yellow isosurface) of the highest occupied orbital (a) and the lowest unoccupied orbital (b) for the gapped configuration (Fig. 1b) at the γ point, demonstrating the valley Hall insulating behavior. C, Mo, and Te atoms are depicted in brown, blue, and green respectively. The insets show as red dots in the band structure the chosen wavefunctions to be plotted. Wavefunctions of the highest occupied orbital (a) (lowest unoccupied orbital (b)) are localized in the C atoms of the top (bottom) layer of graphene, in the carbon atoms that do not sit on top of another carbon atom in the z -direction.

which takes a value $\Delta_E \approx 15$ meV. We note that in this structure no external field is applied, and the opening stems solely from the proximity effect of the ferroelectric. From the DFT calculations, we have also obtained that the size of the electric dipole in the gapped heterostructure is $p = 0.4$ Debye, which leads to an electric bias $\Delta V = 22$ mV between the graphene layers. Note that this bias is two or three orders of magnitude smaller than the one externally applied in AB bilayer graphene devices to obtain the same insulating behavior.^{43,44} In those devices a large screening of the electric voltage occurs in comparison to the bilayer graphene encapsulated in MoTe_2 , where the ferroelectric directly gates the bilayer without screening.

To demonstrate the topological nature of the gap in the insulating configuration, we have computed the wavefunction probability density of the highest occupied and the lowest unoccupied orbitals (see Figs. 2a and 2b and the insets to identify the corresponding wavefunctions). The wavefunctions of the highest occupied orbital are localized in the carbon atoms of the top graphene layer that do not lie on top of the carbon atoms of the other layer in the AB stacking (Fig. 2a). In the case of the lowest unoccupied orbital the wavefunctions are localized in the carbon atoms of the bottom graphene layer that, again, are not aligned with the carbon atoms of the top layer in the AB stacking (Fig. 2b). This feature demonstrates that the gap opening stems from an electrostatic imbalance between the two graphene layers, and not from intervalley scattering in the 3×3 supercell, equivalent to

the effect of an externally applied bias.⁴⁹

B. Low-energy model

We now analyze the emergence of topological excitations in the domain walls that can be created in this ferroelectric heterostructure. To do so, we will effectively describe the bilayer graphene encapsulated in MoTe_2 with a low-energy model. The electronic structure of the heterostructure around the Fermi level can be described with a tight-binding Hamiltonian for AB bilayer graphene, where the effect of the ferroelectric is incorporated through its layer-dependent electrostatic potential.

$$H = t \sum_{\langle ij \rangle} c_i^\dagger c_j + t_I \sum_{ij} \nu_{ij} c_i^\dagger c_j + E \sum_i \beta_i c_i^\dagger c_i, \quad (1)$$

where t is the first neighbor intralayer hopping, t_I is the interlayer hopping, and i and j run over the atomic positions. The term ν_{ij} takes value $\nu_{ij} = 1$ for i, j belonging to different layers and stacked right on top of each other, and $\nu_{ij} = 0$ otherwise. The term β_i takes value $\beta_i = 1$ for the top layer and $\beta_i = -1$ for the bottom layer. Finally, E is the electrostatic difference between the two layers, which depends on the relative configuration of the ferroelectrics. As a reference, the experimental value of the hoppings for graphene bilayers are $t_I \approx 0.15t$, corresponding to $t \approx 3$ eV and $t_I \approx 450$ meV.⁶⁰

Figure 3a shows the band structure for the low energy model (eq. (1)) for $E/t = 0$, this situation corresponds to the heterostructure configuration shown in Fig. 1a, where the net internal interlayer bias induced by the MoTe_2 is zero. We can observe that in the absence of an electric field there is no energy gap, in agreement with the DFT band structure (Fig. 1e). Figure 3b shows the low energy-model band structure for $E/t = 0.1$, this situation corresponds to the heterostructure configuration shown Fig. 1b. In this case, the induced internal interlayer bias in bilayer graphene is non-zero and a gap opens as in Fig. 1f. The local density of states for $E/t = 0.1$ is plotted in Fig. 3c. We can see that the top of the valence band LDOS localizes in the top-layer C atom that does not align with the carbon from the bottom layer. For the bottom of the conduction band LDOS, it localizes in the bottom-layer C atom that does not align with the carbon of the top layer. This result is in agreement with the DFT wavefunction probability density plots shown in Fig. 2, thus confirming the valley Hall insulating character of bilayer graphene encapsulated in MoTe_2 .

Now that we have demonstrated that the low energy model provides a good description of the DFT calculations that we have performed in the heterostructure, we can analyze with it the topological excitations that can emerge. The Berry curvature associated with the energy bands for the insulating case is shown in Fig. 3b. It is observed that the Berry curvature is localized in the K

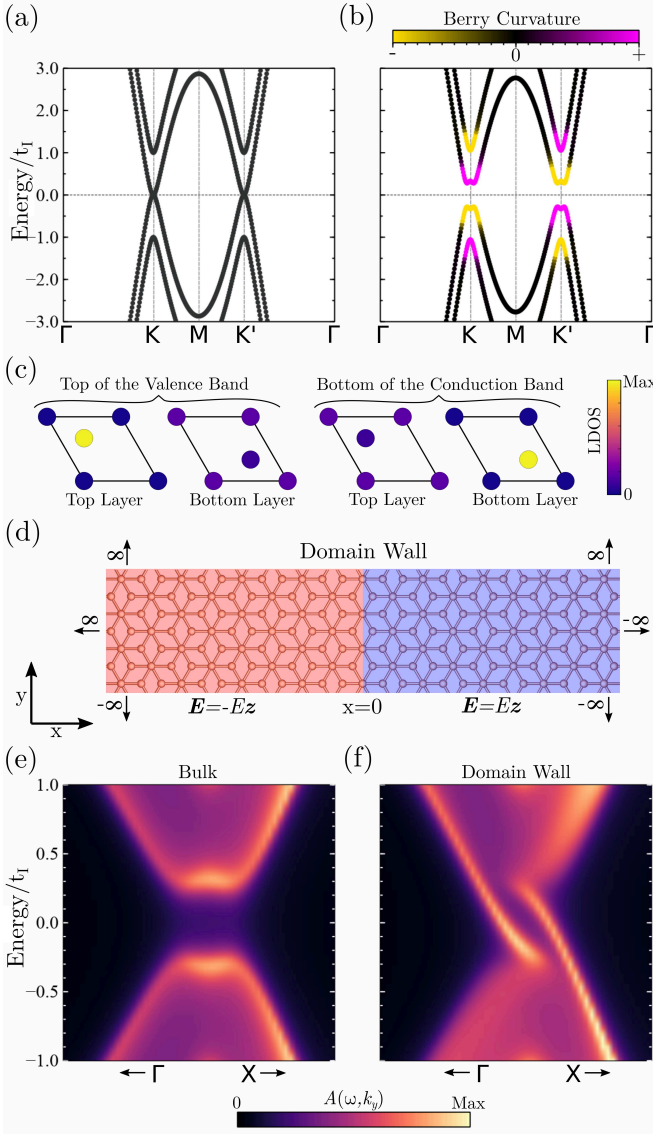


FIG. 3. Low energy model electronic structure of AB bilayer graphene under the absence/presence of an electrostatic bias between layers (eq. (1)) (a) Band structure in the absence of interlayer bias ($E/t = 0$), corresponding to the heterostructure configuration of Fig. 1a. (b) Band structure in the presence of a finite interlayer bias ($E/t = 0.1$), corresponding to the heterostructure configuration of Fig. 1b. The Berry curvature has also been plotted in the bands. (c) Local density of states (LDOS) for $E/t = 0.1$ at the top of the valence band and at the bottom of the conduction band. (d) Schematic of a boundary between different ferroelectric domains (highlighted in red and blue). Both domains display the valley Hall insulating configuration (Fig. 1b), but the electric fields of each domain point in the opposite direction. The domains are semi-infinite in the x direction. The domain wall occurs at $x = 0$. In the y direction the lattice is periodic. (e,f) Momentum resolved spectral function $A(\omega, k_y)$ for the bulk domains (e) and for the domain wall (f).

and K' points, which allows defining a valley Chern num-

ber \mathcal{C}_K and $\mathcal{C}_{K'}$. In the biased bilayer, each valley leads to a Chern number $\mathcal{C}_{K,K'} = \pm 1$, leading to a net valley Chern number $\mathcal{C}_V = \mathcal{C}_K - \mathcal{C}_{K'} = \pm 2$. The existence of a finite valley Chern number gives rise to valley polarized gapless edge modes at the interface between two insulating domains with opposite valley Chern numbers. Figure 3d shows a schematic of a domain wall between two domains (red and blue) in which the electric field E felt by the bilayer has the opposite direction. This corresponds to a situation in which the electric polarization of MoTe₂ layers induces a finite electric field in bilayer graphene, but in each of the domains this field takes the opposite direction. Therefore, the valley Chern numbers take an opposite sign in each of the domains at K and K' . The emergence of interface states is determined by the difference between the corresponding valley Chern numbers at K and K' between red and blue domains. Figures 3e and 3f show the momentum resolved spectral function $A(\omega, k_y)$ for the domain system described in Fig. 3d. We can see that the bulk of both domains remains gapped (Fig. 3e), but at the domain wall (3f) two zero-energy modes emerge as a consequence of the opposite sign that the valley Chern numbers display in each domain.⁴⁹ Interestingly, externally controlling ferroelectric domains allows directly imprinting topological excitations in the heterostructure. Ultimately, the control of the ferroelectric domains allows to use this feature to imprint topological circuits with a ballistic transport behavior in graphene/MoTe₂ heterostructures without requiring to externally apply a bias.

Finally, we discuss the impact of the moiré modulation that emerges due to the mismatch and rotation between bilayer graphene and MoTe₂. Such a moiré modulation arises naturally as a consequence of the lattice-parameter mismatch between MoTe₂ and graphene, and it can be controlled by adjusting the twist angle between the layers of both van der Waals materials. The effect of the moiré modulation can be directly accounted for in the low energy model (eq. (1)), by including a spatially dependent electrostatic potential of the form

$$H_M = \sum_i \epsilon(\mathbf{r}_i) \beta_i c_i^\dagger c_i, \quad (2)$$

where $\epsilon(\mathbf{r}_i) = \epsilon \sum_\alpha \cos\left(\frac{\mathbf{b}_\alpha \cdot \mathbf{r}_i}{n}\right) + C_0$, with \mathbf{b}_α the reciprocal lattice vectors of the moiré unit cell (the summation runs over the 3 \mathbf{b}_α vectors related by C_3 symmetry). The parameter C_0 is taken so that $\langle \epsilon(\mathbf{r}_i) \rangle = 0$. The product $\mathbf{b}_\alpha \cdot \mathbf{r}_i$ equals 2π when \mathbf{r} takes the value of the bilayer graphene lattice vectors, and n is an integer that commensurates the moiré length L_M with the original lattice parameter of graphene a_C as $L_M = na_C$. Therefore, Eq. (2) allows to include a modulated electrostatic potential as the one shown in Fig. 4a in each of the graphene layers. For concreteness, we will analyze the case $L_M = 5a_C$, which corresponds to a 5×5 supercell for graphene,⁶¹ with a well approximated commensurability (less than 1% difference) with MoTe₂. The strength of

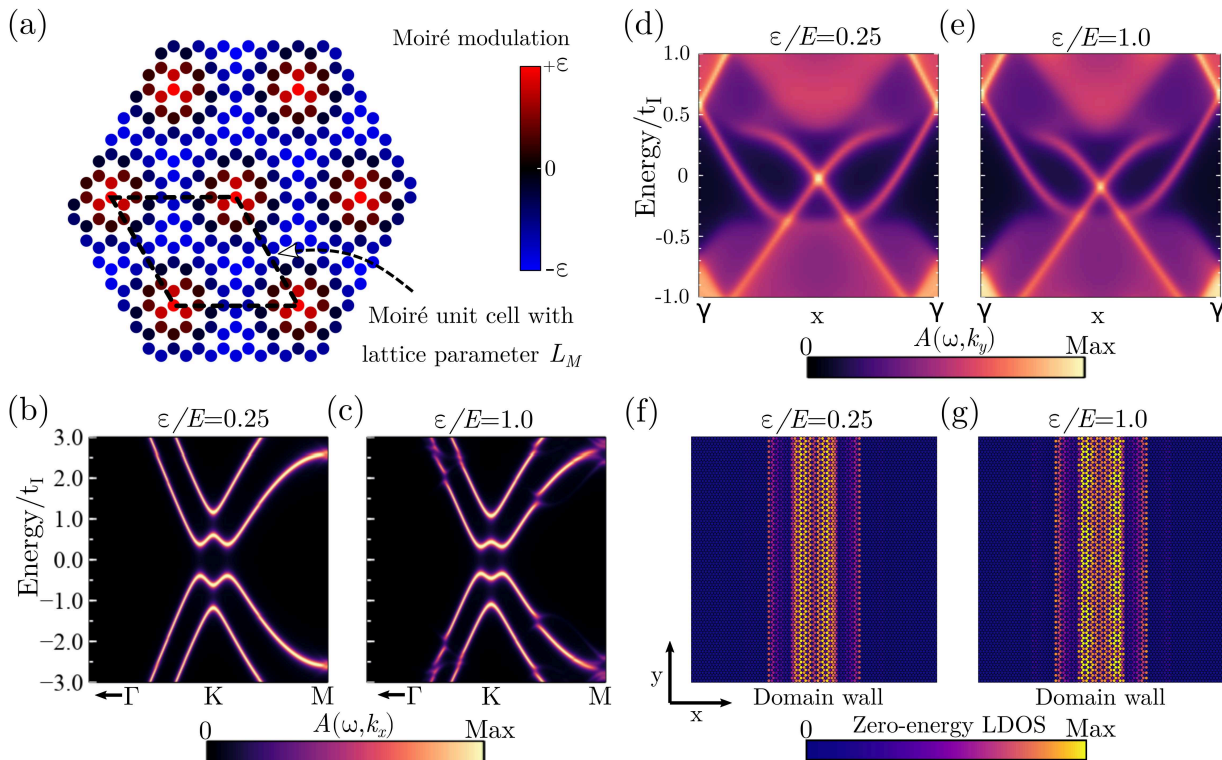


FIG. 4. Calculations including a moiré potential (eq. (2)) in the low energy model of eq. (1) for $E/t = 0.1$. (a) Induced moiré potential by the MoTe₂ in each of the graphene layers. A moiré unit cell emerges on top of the original bilayer graphene unit cell. (b,c) Unfolded momentum resolved spectral functions for $\epsilon/E = 0.25$ (b) and $\epsilon/E = 1.0$ (c). (d,e,f,g) Calculations at the interface between the two ferroelectric domains shown in Fig. 3d, they include the effect of the moiré potential. (d,e) Momentum resolved spectral function for: (d) $\epsilon/E = 0.25$ and (e) and $\epsilon/E = 1.0$. (f,g) Zero-energy local density of states (LDOS) for: (f) $\epsilon/E = 0.25$ and (g) and $\epsilon/E = 1.0$.

the modulation is given by ϵ . We will analyze a moderate modulation of the electric bias $\epsilon/E = 0.25$, and the limit case where the modulation amplitude equals the electric bias $\epsilon/E = 1.0$.

Figures 4b and 4c show the unfolded momentum resolved spectral functions for $\epsilon/E = 0.25$ (4b) and $\epsilon/E = 1.0$ (4c) in the original bilayer graphene unit cell. We can observe the emergence of band anticrossings most noticeable for the strong modulated case ($\epsilon/E = 1.0$). However, the energy gap remains open and barely affected by the moiré modulation. Therefore, we might expect that the valley Hall insulating behavior is robust against possible moiré modulations that might appear between graphene and MoTe₂ layers. To confirm this, Figs. 4d and 4e show the momentum resolved spectral function at the interface between the two ferroelectric domains described in Fig. 3d, this time including the effect of the moiré potential for $\epsilon/E = 0.25$ (Fig. 4d) and $\epsilon/E = 1.0$ (Fig. 4e). Note that in this case the bands have not been unfolded. We can see that zero-energy modes emerge at the interface of the domain walls even for the strongly modulated potential ($\epsilon/E = 1.0$). The effect of the moiré potential in the zero-energy modes can be further rationalized in real space, as shown in Figs. 4f and 4g, where the zero-energy local density of

states (LDOS) is shown at the interface between the two ferroelectric domains described in Fig. 3d. First, it is observed that the zero-energy modes localize at the domain wall, as expected from their in-gap nature. Furthermore, for a strong moiré modulation, ($\epsilon/E = 1.0$, Fig. 4g) the interface modes show a modulation in real space following the moiré potential.^{27,62} It is worth noting that such a moiré modulation does not lead to intervalley scattering, as demonstrated by the gapless nature of the spectral function of Fig. 4d. Therefore, these results demonstrate that the valley Hall insulating character displayed by the graphene-MoTe₂ heterostructure is robust against moiré modulations between the ferroelectric and graphene layers, meaning that a finite misalignment between the layers can exist yielding to the same phenomenology, a feature that dramatically simplifies the experimental design of these heterostructures.

III. CONCLUSIONS

To summarize, we have demonstrated an emergent ferroelectrically-driven valley Hall insulating behavior in AB-stacking bilayer graphene encapsulated in ferroelectric MoTe₂ using a combination of *ab initio* calcula-

tions and low-energy models. First-principles calculations show how the gap in bilayer graphene can be opened and closed as a function of the orientation between the two layers of MoTe₂. For opposite ferroelectric polarization between the MoTe₂ encapsulation, the net effective field felt by bilayer graphene is zero and hence the system remains gapless. When the electric polarizations of both MoTe₂ layers point in the same direction, a non-zero electric field is induced in graphene bilayer, thus producing a valley Hall insulating behavior. Furthermore, we demonstrated that moiré modulations of the electrostatic bias created by the ferroelectric do not impact the valley Hall insulating character of the heterostructure, and topological modes are robust to it. Our results put forward ferroelectric/graphene heterostructures as versatile valves with a built-in electrostatically controlled topolog-

ical electronic structure. Ultimately, the built-in electric fields of these heterostructures would allow creating a wide variety of permanent electrically defined quantum dots architectures and biased twisted graphene multilayers, without requiring the application of external biases.

ACKNOWLEDGEMENTS

We acknowledge the computational resources provided by the Aalto Science-IT project, and the financial support from the Academy of Finland Projects No. 331342, No. 336243 and No. 349696 and the Jane and Aatos Erkko Foundation. We thank P. Liljeroth, M. Amini and S. Kezilebieke for useful discussions.

-
- ¹ A. K. Geim and I. V. Grigorieva, “Van der waals heterostructures,” *Nature* **499**, 419–425 (2013).
 - ² Ahmed Abouelkomsan, Zhao Liu, and Emil J. Bergholtz, “Particle-hole duality, emergent fermi liquids, and fractional chern insulators in moiré flatbands,” *Phys. Rev. Lett.* **124**, 106803 (2020).
 - ³ Cécile Repellin and T. Senthil, “Chern bands of twisted bilayer graphene: Fractional chern insulators and spin phase transition,” *Phys. Rev. Research* **2**, 023238 (2020).
 - ⁴ Yonglong Xie, Andrew T. Pierce, Jeong Min Park, Daniel E. Parker, Eslam Khalaf, Patrick Ledwith, Yuan Cao, Seung Hwan Lee, Shaowen Chen, Patrick R. Forrester, Kenji Watanabe, Takashi Taniguchi, Ashvin Vishwanath, Pablo Jarillo-Herrero, and Amir Yacoby, “Fractional chern insulators in magic-angle twisted bilayer graphene,” *Nature* **600**, 439–443 (2021).
 - ⁵ Saptarshi Das, Hong-Yan Chen, Ashish Verma Penu-matcha, and Joerg Appenzeller, “High performance multilayer mos₂ transistors with scandium contacts,” *Nano Letters* **13**, 100–105 (2012).
 - ⁶ Qing Hua Wang, Kouros Kalantar-Zadeh, Andras Kis, Jonathan N. Coleman, and Michael S. Strano, “Electronics and optoelectronics of two-dimensional transition metal dichalcogenides,” *Nature Nanotechnology* **7**, 699–712 (2012).
 - ⁷ Hee Sung Lee, Seung Su Baik, Kimoon Lee, Sung-Wook Min, Pyo Jin Jeon, Jin Sung Kim, Kyujin Choi, Hyoung Joon Choi, Jae Hoon Kim, and Seongil Im, “Metal semiconductor field-effect transistor with mos₂/conducting nio_{x-1} van der waals schottky interface for intrinsic high mobility and photoswitching speed,” *ACS Nano* **9**, 8312–8320 (2015).
 - ⁸ Guangyi Chen, Shaomian Qi, Jianqiao Liu, Di Chen, Jiongjie Wang, Shili Yan, Yu Zhang, Shimin Cao, Ming Lu, Shibing Tian, Kangyao Chen, Peng Yu, Zheng Liu, X. C. Xie, Jiang Xiao, Ryuichi Shindou, and Jian-Hao Chen, “Electrically switchable van der waals magnon valves,” *Nature Communications* **12**, 6279 (2021).
 - ⁹ Hailong Lin, Faguang Yan, Ce Hu, Quanshan Lv, Wenkai Zhu, Ziao Wang, Zhongming Wei, Kai Chang, and Kaiyou Wang, “Spin-valve effect in fe₃gete₂/mos₂/fe₃gete₂van der waals heterostructures,” *ACS Applied Materials Interfaces* **12**, 43921–43926 (2020).
 - ¹⁰ C. Cardoso, D. Soriano, N. A. García-Martínez, and J. Fernández-Rossier, “Van der waals spin valves,” *Phys. Rev. Lett.* **121**, 067701 (2018).
 - ¹¹ Jae-Ung Lee, Sungmin Lee, Ji Hoon Ryoo, Soonmin Kang, Tae Yun Kim, Pilkwang Kim, Cheol-Hwan Park, Je-Geun Park, and Hyeonsik Cheong, “Ising-type magnetic ordering in atomically thin fep₃,” *Nano Letters* **16**, 7433–7438 (2016).
 - ¹² Bevin Huang, Genevieve Clark, Efrén Navarro-Moratalla, Dahlia R. Klein, Ran Cheng, Kyle L. Seyler, Ding Zhong, Emma Schmidgall, Michael A. McGuire, David H. Cobden, Wang Yao, Di Xiao, Pablo Jarillo-Herrero, and Xiaodong Xu, “Layer-dependent ferromagnetism in a van der waals crystal down to the monolayer limit,” *Nature* **546**, 270–273 (2017).
 - ¹³ Cheng Gong, Lin Li, Zhenglu Li, Huiwen Ji, Alex Stern, Yang Xia, Ting Cao, Wei Bao, Chenzhe Wang, Yuan Wang, Z. Q. Qiu, R. J. Cava, Steven G. Louie, Jing Xia, and Xiang Zhang, “Discovery of intrinsic ferromagnetism in two-dimensional van der waals crystals,” *Nature* **546**, 265–269 (2017).
 - ¹⁴ Zaiyao Fei, Bevin Huang, Paul Malinowski, Wenbo Wang, Tiancheng Song, Joshua Sanchez, Wang Yao, Di Xiao, Xi-aoyang Zhu, Andrew F. May, Weida Wu, David H. Cobden, Jiun-Haw Chu, and Xiaodong Xu, “Two-dimensional itinerant ferromagnetism in atomically thin fe₃gete₂,” *Nature Materials* **17**, 778–782 (2018).
 - ¹⁵ Zhaowei Zhang, Jingzhi Shang, Chongyun Jiang, Abdullah Rasmita, Weibo Gao, and Ting Yu, “Direct photoluminescence probing of ferromagnetism in monolayer two-dimensional crbr₃,” *Nano Letters* **19**, 3138–3142 (2019).
 - ¹⁶ Miguel M. Ugeda, Aaron J. Bradley, Yi Zhang, Seitai Onishi, Yi Chen, Wei Ruan, Claudia Ojeda-Aristizabal, Hye-jin Ryu, Mark T. Edmonds, Hsin-Zon Tsai, and et al., “Characterization of collective ground states in single-layer nbse₂,” *Nature Physics* **12**, 92–97 (2015).
 - ¹⁷ Shuoguo Yuan, Xin Luo, Hung Lit Chan, Chengcheng Xiao, Yawei Dai, Maohai Xie, and Jianhua Hao, “Room-temperature ferroelectricity in mote₂ down to the atomic monolayer limit,” *Nature Communications* **10**, 1775 (2019).

- ¹⁸ Qian Song, Connor A. Occhialini, Emre Ergeçen, Batyr Ilyas, Danila Amoroso, Paolo Barone, Jesse Kapeghian, Kenji Watanabe, Takashi Taniguchi, Antia S. Botana, Silvia Picozzi, Nuh Gedik, and Riccardo Comin, “Evidence for a single-layer van der waals multiferroic,” *Nature* **602**, 601–605 (2022).
- ¹⁹ Adolfo O Fumega and J L Lado, “Microscopic origin of multiferroic order in monolayer NiI₂,” *2D Materials* **9**, 025010 (2022).
- ²⁰ D. R. Klein, D. MacNeill, J. L. Lado, D. Soriano, E. Navarro-Moratalla, K. Watanabe, T. Taniguchi, S. Manni, P. Canfield, J. Fernández-Rossier, and P. Jarillo-Herrero, “Probing magnetism in 2d van der waals crystalline insulators via electron tunneling,” *Science* **360**, 1218–1222 (2018).
- ²¹ Shengwei Jiang, Lizhong Li, Zefang Wang, Jie Shan, and Kin Fai Mak, “Spin tunnel field-effect transistors based on two-dimensional van der waals heterostructures,” *Nature Electronics* **2**, 159–163 (2019).
- ²² Baozeng Zhou, Shiwen Ji, Zhen Tian, Weijia Cheng, Xiaocha Wang, and Wenbo Mi, “Proximity effect induced spin filtering and gap opening in graphene by half-metallic monolayer cr₂c ferromagnet,” *Carbon* **132**, 25–31 (2018).
- ²³ Shengmei Qi, Jiawei Jiang, Xiaocha Wang, and Wenbo Mi, “Valley polarization, magnetic anisotropy and dzyaloshinskii-moriya interaction of two-dimensional graphene/janus 2h-vsex (x = s, te) heterostructures,” *Carbon* **174**, 540–555 (2021).
- ²⁴ Sobhit Singh, Camilo Espejo, and Aldo H. Romero, “Structural, electronic, vibrational, and elastic properties of graphene/mos₂ bilayer heterostructures,” *Phys. Rev. B* **98**, 155309 (2018).
- ²⁵ Thomas Naimer, Klaus Zollner, Martin Gmitra, and Jaroslav Fabian, “Twist-angle dependent proximity induced spin-orbit coupling in graphene/transition metal dichalcogenide heterostructures,” *Phys. Rev. B* **104**, 195156 (2021).
- ²⁶ Shawulienu Kezilebieke, Md Nurul Huda, Viliam Vaño, Markus Aapro, Somesh C. Ganguli, Orlando J. Silveira, Szczepan Głodzik, Adam S. Foster, Teemu Ojanen, and Peter Liljeroth, “Topological superconductivity in a van der waals heterostructure,” *Nature* **588**, 424–428 (2020).
- ²⁷ Shawulienu Kezilebieke, Viliam Vaño, Md N. Huda, Markus Aapro, Somesh C. Ganguli, Peter Liljeroth, and Jose L. Lado, “Moiré-enabled topological superconductivity,” *Nano Letters* **22**, 328–333 (2022).
- ²⁸ Livio Ciorciaro, Martin Kroner, Kenji Watanabe, Takashi Taniguchi, and Atac Imamoglu, “Observation of magnetic proximity effect using resonant optical spectroscopy of an electrically tunable mose₂/crbr₃ heterostructure,” *Phys. Rev. Lett.* **124**, 197401 (2020).
- ²⁹ T. P. Lyons, D. Gillard, A. Molina-Sánchez, A. Misra, F. Withers, P. S. Keatley, A. Kozikov, T. Taniguchi, K. Watanabe, K. S. Novoselov, J. Fernández-Rossier, and A. I. Tartakovskii, “Interplay between spin proximity effect and charge-dependent exciton dynamics in MoSe₂/CrBr₃ van der waals heterostructures,” *Nature Communications* **11** (2020), 10.1038/s41467-020-19816-4.
- ³⁰ Viliam Vaño, Mohammad Amini, Somesh C. Ganguli, Guangze Chen, Jose L. Lado, Shawulienu Kezilebieke, and Peter Liljeroth, “Artificial heavy fermions in a van der waals heterostructure,” *Nature* **599**, 582–586 (2021).
- ³¹ Wen Wan, Rishav Harsh, Antonella Meninno, Paul Dreher, Sandra Sajan, Ion Errea, Fernando de Juan, and Miguel M. Ugeda, “Magnetic order in a coherent two-dimensional Kondo lattice,” arXiv e-prints, arXiv:2207.00096 (2022), arXiv:2207.00096 [cond-mat.str-el].
- ³² Dahlia R. Klein, Li-Qiao Xia, David MacNeill, Kenji Watanabe, Takashi Taniguchi, and Pablo Jarillo-Herrero, “Electrical switching of a moiré ferroelectric superconductor,” arXiv e-prints, arXiv:2205.04458 (2022), arXiv:2205.04458 [cond-mat.supr-con].
- ³³ M. Vizner Stern, Y. Waschitz, W. Cao, I. Nevo, K. Watanabe, T. Taniguchi, E. Sela, M. Urbakh, O. Hod, and M. Ben Shalom, “Interfacial ferroelectricity by van der waals sliding,” *Science* **372**, 1462–1466 (2021).
- ³⁴ Fei Xue, Jr-Hau He, and Xixiang Zhang, “Emerging van der waals ferroelectrics: Unique properties and novel devices,” *Applied Physics Reviews* **8**, 021316 (2021).
- ³⁵ Antimo Marrazzo and Marco Gibertini, “Twist-resilient and robust ferroelectric quantum spin hall insulators driven by van der waals interactions,” *npj 2D Materials and Applications* **6** (2022), 10.1038/s41699-022-00305-9.
- ³⁶ Mengwei Si, Atanu K. Saha, Shengjie Gao, Gang Qiu, Jingkai Qin, Yuqin Duan, Jie Jian, Chang Niu, Haiyan Wang, Wenzhuo Wu, Sumeet K. Gupta, and Peide D. Ye, “A ferroelectric semiconductor field-effect transistor,” *Nature Electronics* **2**, 580–586 (2019).
- ³⁷ Yan Chen, Xudong Wang, Le Huang, Xiaoting Wang, Wei Jiang, Zhen Wang, Peng Wang, Binmin Wu, Tie Lin, Hong Shen, Zhongming Wei, Weida Hu, Xiangjian Meng, Junhao Chu, and Jianlu Wang, “Ferroelectric-tuned van der waals heterojunction with band alignment evolution,” *Nature Communications* **12** (2021), 10.1038/s41467-021-24296-1.
- ³⁸ Yuan Cao, Valla Fatemi, Ahmet Demir, Shiang Fang, Spencer L. Tomarken, Jason Y. Luo, Javier D. Sanchez-Yamagishi, Kenji Watanabe, Takashi Taniguchi, Efthimios Kaxiras, Ray C. Ashoori, and Pablo Jarillo-Herrero, “Correlated insulator behaviour at half-filling in magic-angle graphene superlattices,” *Nature* **556**, 80–84 (2018).
- ³⁹ Yuan Cao, Valla Fatemi, Shiang Fang, Kenji Watanabe, Takashi Taniguchi, Efthimios Kaxiras, and Pablo Jarillo-Herrero, “Unconventional superconductivity in magic-angle graphene superlattices,” *Nature* **556**, 43–50 (2018).
- ⁴⁰ Aaron L. Sharpe, Eli J. Fox, Arthur W. Barnard, Joe Finney, Kenji Watanabe, Takashi Taniguchi, M. A. Kastner, and David Goldhaber-Gordon, “Emergent ferromagnetism near three-quarters filling in twisted bilayer graphene,” *Science* **365**, 605–608 (2019), <https://www.science.org/doi/pdf/10.1126/science.aaw3780>.
- ⁴¹ M. Serlin, C. L. Tschirhart, H. Polshyn, Y. Zhang, J. Zhu, K. Watanabe, T. Taniguchi, L. Balents, and A. F. Young, “Intrinsic quantized anomalous hall effect in a moiré heterostructure,” *Science* **367**, 900–903 (2020), <https://www.science.org/doi/pdf/10.1126/science.aay5533>.
- ⁴² Youngjoon Choi, Hyunjin Kim, Yang Peng, Alex Thomson, Cyprian Lewandowski, Robert Polski, Yiran Zhang, Harpreet Singh Arora, Kenji Watanabe, Takashi Taniguchi, Jason Alicea, and Stevan Nadj-Perge, “Correlation-driven topological phases in magic-angle twisted bilayer graphene,” *Nature* **589**, 536–541 (2021).
- ⁴³ Eduardo V. Castro, K. S. Novoselov, S. V. Morozov, N. M. R. Peres, J. M. B. Lopes dos Santos, Johan Nilsson, F. Guinea, A. K. Geim, and A. H. Castro Neto, “Biased bilayer graphene: Semiconductor with a gap tunable by the electric field effect,” *Phys. Rev. Lett.* **99**, 216802

- (2007).
- ⁴⁴ Jeroen B. Oostinga, Hubert B. Heersche, Xinglan Liu, Alberto F. Morpurgo, and Lieven M. K. Vandersypen, “Gate-induced insulating state in bilayer graphene devices,” *Nature Materials* **7**, 151–157 (2008).
- ⁴⁵ Yuanbo Zhang, Tsung-Ta Tang, Caglar Girit, Zhao Hao, Michael C. Martin, Alex Zettl, Michael F. Crommie, Y. Ron Shen, and Feng Wang, “Direct observation of a widely tunable bandgap in bilayer graphene,” *Nature* **459**, 820–823 (2009).
- ⁴⁶ Fengnian Xia, Damon B. Farmer, Yu ming Lin, and Phaedon Avouris, “Graphene field-effect transistors with high on/off current ratio and large transport band gap at room temperature,” *Nano Letters* **10**, 715–718 (2010).
- ⁴⁷ Marius Eich, František Herman, Riccardo Pisoni, Hiske Overweg, Annika Kurzmann, Yongjin Lee, Peter Rickhaus, Kenji Watanabe, Takashi Taniguchi, Manfred Sigrist, Thomas Ihn, and Klaus Ensslin, “Spin and valley states in gate-defined bilayer graphene quantum dots,” *Phys. Rev. X* **8**, 031023 (2018).
- ⁴⁸ Haoxin Zhou, Ludwig Holleis, Yu Saito, Liam Cohen, William Huynh, Caitlin L. Patterson, Fangyuan Yang, Takashi Taniguchi, Kenji Watanabe, and Andrea F. Young, “Isospin magnetism and spin-polarized superconductivity in bernal bilayer graphene,” *Science* **375**, 774–778 (2022).
- ⁴⁹ Ivar Martin, Ya. M. Blanter, and A. F. Morpurgo, “Topological confinement in bilayer graphene,” *Phys. Rev. Lett.* **100**, 036804 (2008).
- ⁵⁰ Long Ju, Zhiwen Shi, Nityan Nair, Yinchuan Lv, Chenhao Jin, Jairo Velasco, Claudia Ojeda-Aristizabal, Hans A. Bechtel, Michael C. Martin, Alex Zettl, James Analytis, and Feng Wang, “Topological valley transport at bilayer graphene domain walls,” *Nature* **520**, 650–655 (2015).
- ⁵¹ Fan Zhang, Allan H. MacDonald, and Eugene J. Mele, “Valley chern numbers and boundary modes in gapped bilayer graphene,” *Proceedings of the National Academy of Sciences* **110**, 10546–10551 (2013).
- ⁵² Abolhassan Vaezi, Yufeng Liang, Darryl H. Ngai, Li Yang, and Eun-Ah Kim, “Topological edge states at a tilt boundary in gated multilayer graphene,” *Phys. Rev. X* **3**, 021018 (2013).
- ⁵³ Zhenhua Qiao, Jeil Jung, Qian Niu, and Allan H. MacDonald, “Electronic highways in bilayer graphene,” *Nano Letters* **11**, 3453–3459 (2011).
- ⁵⁴ Jing Li, Ke Wang, Kenton J. McFaul, Zachary Zern, Yafei Ren, Kenji Watanabe, Takashi Taniguchi, Zhenhua Qiao, and Jun Zhu, “Gate-controlled topological conducting channels in bilayer graphene,” *Nature Nanotechnology* **11**, 1060–1065 (2016).
- ⁵⁵ Peter Rickhaus, John Wallbank, Sergey Slizovskiy, Riccardo Pisoni, Hiske Overweg, Yongjin Lee, Marius Eich, Ming-Hao Liu, Kenji Watanabe, Takashi Taniguchi, Thomas Ihn, and Klaus Ensslin, “Transport through a network of topological channels in twisted bilayer graphene,” *Nano Letters* **18**, 6725–6730 (2018).
- ⁵⁶ P. Hohenberg and W. Kohn, “Inhomogeneous electron gas,” *Phys. Rev.* **136**, B864–B871 (1964).
- ⁵⁷ An alternative ratio between the lattice parameters of pristine graphene and MoTe₂ would be 5×5 supercells of graphene embedded in 2×2 supercells of MoTe₂. We analyze in the next section the effect that such 5×5 modulation creates in the electronic properties of the heterostructure.
- ⁵⁸ Paolo Giannozzi *et al.*, “Quantum espresso: a modular and open-source software project for quantum simulations of materials,” *J. Phys. Condens. Matter* **21**, 395502 (2009).
- ⁵⁹ Paolo Giannozzi *et al.*, “Advanced capabilities for materials modelling with quantum espresso,” *Journal of Physics: Condensed Matter* **29**, 465901 (2017).
- ⁶⁰ A. H. Castro Neto, F. Guinea, N. M. R. Peres, K. S. Novoselov, and A. K. Geim, “The electronic properties of graphene,” *Rev. Mod. Phys.* **81**, 109–162 (2009).
- ⁶¹ We have checked that the phenomenology presented here is robust against other modulations different from the 5×5.
- ⁶² Maryam Khosravian and Jose L. Lado, “Impurity-induced excitations in a topological two-dimensional ferromagnet/superconductor van der Waals moiré heterostructure,” *Phys. Rev. Mater.* **6**, 094010 (2022).